Thermodynamic Cycle Analysis and Inhibitor Design against Beta-Lactamase[†]

Tomer A. Roth,[#,‡] George Minasov,[#,§] Stefania Morandi,[⊥] Fabio Prati,[⊥] and Brian K. Shoichet*,[#]

Department of Pharmaceutical Chemistry, University of California San Francisco, 600 16th Street, San Francisco, California 94143-2240, and Dipartimento di Chimica, Universitá degli studi di Modena e Reggio Emilia, via Campi 183, Modena, Italy

ABSTRACT: β-Lactamases are the most widespread resistance mechanism to β-lactam antibiotics, such as the penicillins and cephalosporins. Transition-state analogues that bind to the enzymes with nanomolar affinities have been introduced in an effort to reverse the resistance conferred by these enzymes. To understand the origins of this affinity, and to guide design of future inhibitors, double-mutant thermodynamic cycle experiments were undertaken. An unexpected hydrogen bond between the nonconserved Asn289 and a key inhibitor carboxylate was observed in the X-ray crystal structure of a 1 nM inhibitor (compound **1**) in complex with AmpC β-lactamase. To investigate the energy of this hydrogen bond, the mutant enzyme N289A was made, as was an analogue of **1** that lacked the carboxylate (compound **2**). The differential affinity of the four different protein and analogue complexes indicates that the carboxylate−amide hydrogen bond contributes 1.7 kcal/mol to overall binding affinity. Synthesis of an analogue of **1** where the carboxylate was replaced with an aldehyde led to an inhibitor that lost all this hydrogen bond energy, consistent with the importance of the ionic nature of this hydrogen bond. To investigate the structural bases of these energies, X-ray crystal structures of N289A/**1** and N289A/**2** were determined to 1.49 and 1.39 Å, respectively. These structures suggest that no significant rearrangement occurs in the mutant versus the wild-type complexes with both compounds. The mutant enzymes L119A and L293A were made to investigate the interaction between a phenyl ring in **1** and these residues. Whereas deletion of the phenyl itself diminishes affinity by 5-fold, the double-mutant cycles suggest that this energy does not come through interaction with the leucines, despite the close contact in the structure. The energies of these interactions provide key information for the design of improved inhibitors against β-lactamases. The high magnitude of the ion−dipole interaction between Asn289 and the carboxylate of **1** is consistent with the idea that ionic interactions can provide significant net affinity in inhibitor complexes.

The proliferation of antibiotic resistant bacteria has become a major public health problem (*1−3*). Among the most pernicious resistance mechanisms are β-lactamas enzymes, which inactivate β-lactam antibiotics, such as penicillins and cephalosporins (*4*). To combat β-lactamases, inhibitors of these enzymes, such as clavulanic acid, can be administered alongside a primary β-lactam antibiotic; these inhibitors have found wide clinical use (*5*). Because these inhibitors are themselves β-lactams, they are susceptible to the bacterial defense mechanisms that have evolved over evolutionary time to counter the primary β-lactam antibiotics. These β-lactam-based β-lactamase inhibitors can have their access blocked by porin channel mutations, they may be hydrolyzed by mutant β-lactamases, and they can upregulate the expression of the very β-lactamases they are meant to inhibit. Thus,

there is a need for novel, non-β-lactam inhibitors of these enzymes.

Non-β-lactam inhibitors of β-lactamase based on boronic acids have shown promise as possible leads for drug discovery (*6−10*). These inhibitors form reversible covalent bonds with the enzyme's catalytic serine and act as transition-state analogues of the deacylation step of the hydrolysis reaction. As these inhibitors have come to increasingly resemble the substrates, their affinity has improved to the point where they can inhibit the enzymes with K_i values as low as 1 nM and can reverse β-lactam resistance in bacterial culture (*9*, *10*).

Previously, we had designed a 1 nM inhibitor of AmpC β-lactamase that was based on the β-lactam antibiotic cephalothin (compound **1**, Figure 1a) (*10*). The benzoic acid group of **1** was intended to mimic the dihydrothiazine ring system of cephalothin and duplicate the position of the C4′-carboxylate in the active site (Figure 1b). All β-lactams bear negatively charged groups at this position, and structural analysis of the binding determinants of AmpC suggests that there is a complementary carboxylate binding site on the enzyme (*11*). Among known structures of AmpC with bound substrate, the analagous carboxylate hydrogen bonds with either Asn343 or Asn346 (*12−14*). Thus, it was expected that the carboxylate of **1** would hydrogen bond with at least one of those residues.

* Corresponding author. E-mail: shoichet@cgl.ucsf.edu; phone: 415−514−4126; fax: 415−302−1411.

University of California San Francisco.

⊥ Universitá degli studi di Modena e Reggio Emilia.

‡ Current Address: Feinberg School of Medicine, Northwestern University, 303 East Chicago Avenue, Chicago, IL 60611.

§ Current Address: Department of Molecular Pharmacology and Biological Chemistry, Northwestern University, 303 East Chicago Avenue, Chicago, IL 60611.
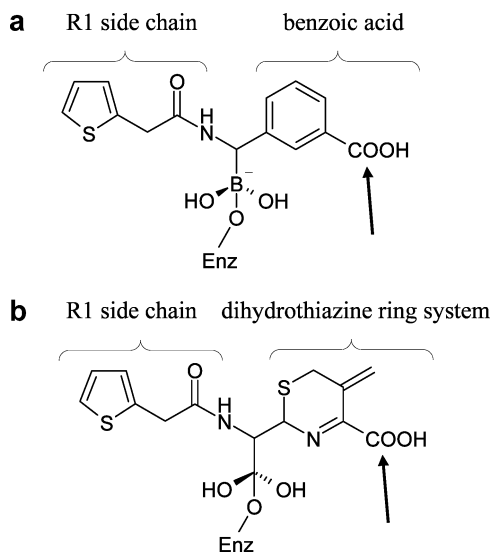
FIGURE 1: Comparison of the covalent adduct of (a) compound **1**, with (b) the high energy intermediate of the substrate cephalothin. Arrows indicate the carboxylate of interest.
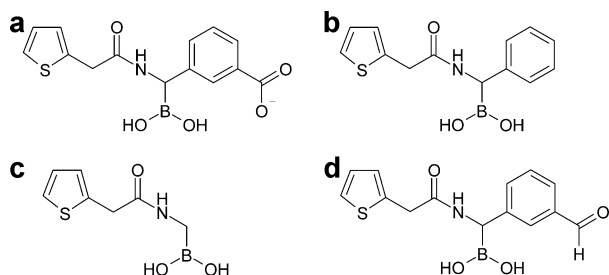

FIGURE 2: Comparison of (a) compound **1**, a 1 nM inhibitor of AmpC, (b) compound **2**, a 35 nM inhibitor of AmpC, (c) compound **3**, a 186 nM inhibitor of AmpC, and (d) compound **8**, a 15 nM inhibitor of AmpC.

Surprisingly, the crystal structure of **1** in complex with AmpC revealed a hydrogen bond between the *m*-carboxylate of the benzoic acid and Asn289 (*10*), and not Asn343 or Asn346, as we had expected and designed. In addition to this unique hydrogen bond, the phenyl ring of the benzoic acid makes van der Waals contacts with both Leu119 and Leu293, which form a hydrophobic patch within the active site (*11*). Comparison of **1** with two similar inhibitors (compounds **2** and **3**, Figure 2b,c) suggests that both the phenyl ring and the *m*-carboxylate of the benzoic acid contribute to the high affinity of **1**. The absence of the *m*-carboxylate in compound **2** decreases inhibitor affinity 35-fold (2.1 kcal/mol) (*10*). The further removal of the phenyl ring in compound **3** (*9*) results in another 5-fold drop in affinity to 186 nM (3.1 kcal/mol overall drop from **1**).

Although it is clear from the structure of **1**/AmpC that the benzoic acid hydrogen bonds with Asn289 and makes hydrophobic contacts with both Leu119 and Leu293, the energies of these interactions were unknown. For instance, the carboxylate improves **1**'s binding energy by 2.1 kcal/mol, but it was unclear how much of this energy is specifically derived from the hydrogen bond with Asn289. This binding energy could alternatively result from ionic interactions between the carboxylate and positively charged protein residues, or through hydrogen bonds with ordered water molecules. The fact that Asn289 is poorly conserved among class C β-lactamases casts further doubt on the
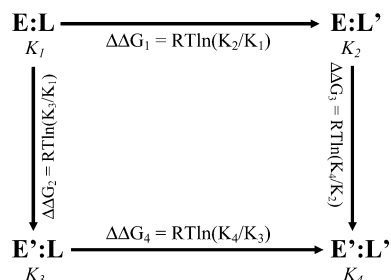

FIGURE 3: General double perturbation thermodynamic cycle. E = wild-type enzyme, E' = mutant enzyme. L = wild-type ligand, L' = "mutant" ligand. $\Delta\Delta\Delta G = (\Delta\Delta G_1 - \Delta\Delta G_4)$ or $(\Delta\Delta G_2 - \Delta\Delta G_3)$.

importance of this crystallographically observed interaction. Quantitative knowledge of the energy of these interactions is vital to the design of future derivatives of **1**, as those interactions critical to the high affinity of the lead compound should be preserved in any future iteration.

One way to quantify this interaction energy is through the use of thermodynamic cycles. Such cycles can be used through double mutant perturbations to study the direct interactions between individual amino acids during protein folding, enzyme catalysis (*15*), protein−protein binding (*16−18*), and ion channel function (*19*). Similarly, it is possible to use thermodynamic cycles to study the interaction between a functional group of a ligand and an active site residue (*20−22*). These experiments use wild-type and "mutant" versions of both the enzyme and ligand, with each "mutant" lacking the interacting groups of interest. The energetic cost, $\Delta\Delta G$, of removing the ligand functional group both in the presence and the absence of the residue with which it interacts can be calculated, and the difference between these energies, $\Delta\Delta\Delta G$, is the energy of the interaction (Figure 3). In these experiments, analogue ("mutant") forms of the ligand must be synthesized, and for drug-like organic molecules this is rarely as straightforward as making a site substitution in a protein. This might explain why this sort of analysis is rarely used in drug-design efforts, even though it is the surest path to understanding what interactions are important for affinity.

To quantify the energetic contributions of the hydrogen bond with Asn289 and the hydrophobic contacts with Leu119 and Leu293, we prepared three separate double-perturbation thermodynamic cycles. K_i values for all four possible enzyme−ligand combinations were used to calculate $\Delta\Delta G$ values for transitions between each complex. To determine the energy of the hydrogen bond, the thermodynamic cycle **A** was set up with **1** as the "wild-type" ligand, and **2** as the "mutant" ligand (Figure 4a). In this cycle, AmpC N289A was used as the mutant enzyme. To determine the energies of the phenyl ring interactions with both Leu119 and Leu293, two separate thermodynamic cycles **B** and **C** were set up with AmpC L119A and L293A as the respective mutant enzymes (Figure 4b,c). In both of these cycles, **2** was considered the "wild-type" ligand, and **3** the "mutant" ligand. To give these energetic studies a detailed structural context, X-ray crystal structures of N289A in complex with both **1** and **2** were determined to 1.49 and 1.39 Å, respectively.

MATERIALS AND METHODS

Enzyme Mutagenesis and Preparation. Mutants of AmpC were created using the overlap extension polymerase chain
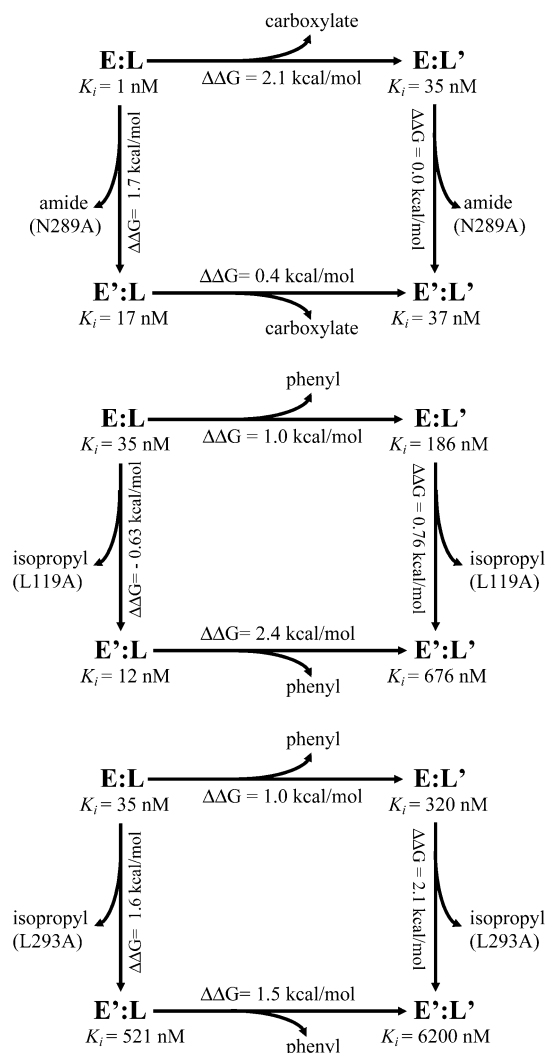
FIGURE 4: (a) Thermodynamic cycle to quantify the hydrogen bond energy between Asn289 and the inhibitor carboxylate. E = wild-type AmpC, E′ = AmpC N289A. L = compound **1**, L′ = compound **2**. $\Delta\Delta\Delta G$ = 1.7 kcal/mol. (b) Thermodynamic cycle to quantify the interaction between the inhibitor phenyl ring and Leu119. E = wild-type AmpC, E′ = AmpC L119A. L = compound **2**, L′ = compound **3**. $\Delta\Delta\Delta G$ = − 1.4 kcal/mol. (c) Thermodynamic cycle to quantify the interaction between the inhibitor phenyl ring and Leu293. E = wild-type AmpC, E′ = AmpC L293A. L = compound **2**, L′ = compound **3**. $\Delta\Delta\Delta G$ = −0.5 kcal/mol.

reaction (*23*). Mutant enzymes were expressed as described (*6*, *13*). AmpC N289A and L293A were purified on an *m*-aminophenylboronic acid affinity column (*6*). AmpC L119A was purified on an S-Sepharose ion-exchange column (*13*). The purified enzymes were concentrated using Centricon spin concentrators.

Enzymology. The glycylboronic acids were dissolved in DMSO[1] at a concentration of 50 mM; more dilute stocks were subsequently prepared as necessary. Kinetic measurements were performed using nitrocefin as a substrate in 50 mM Tris buffer, pH 7.0, and monitored at 480 nm in an HP9453 UV−vis spectrophotometer. To prevent overestimation of inhibition due to sequestration of the enzyme on the

---

walls of the cuvette during the reaction, 0.1% BSA was added to the buffer in all reactions. The K_M values of nitrocefin for L119A, N289A, and L293A were 308, 27, and 33 μM respectively; the value for the wild-type enzyme is 127 μM. To determine K_i values, inhibitor and enzyme were incubated together in the cuvettes for 5 min before reaction was initiated by the addition of substrate. A 200 μM nitrocefin concentration was used for the reactions with L119A and L293A, whereas 400 μM nitrocefin was used for the reactions with N289A to shorten the lag phase of the reaction. For the reactions with N289A, rates were calculated from the later portions of the curve, once the reactions had achieved steady state. These rates were compared with portions of the uninhibited curves that corresponded to the same range of substrate concentrations. K_i values were calculated using the progress curve method described by Waley (*24*), which has been used extensively for boronic acid inhibitors of β-lactamase (*7*, *9*).

Crystal Growth and Structure Determination. Cocrystals of AmpC N289A in complex with compounds **1** and **2** were grown by vapor diffusion in hanging drops equilibrated over 1.7 M potassium phosphate buffer (pH 8.7) using microseeding techniques (*9*, *14*). The initial concentration of the protein in the drop was 3.8 mg/mL and the concentration of compounds **1** and **2** was 588 μM. The compounds were added to the drop in a 1.2% DMSO, 1 M potassium phosphate buffer (pH 8.7) solution. Crystals appeared 5−7 days after equilibration at 23 °C. Before data collection, crystals were immersed in a cryoprotectant solution of 23% sucrose, 1.7 M potassium phosphate, pH 8.7, for about 30 s, and were flash cooled in liquid nitrogen. Data were measured on the DND-CAT beam line (5IDB) of the Advanced Photon Source at Argonne National Laboratory at 100 K using a Mar-CCD detector. Both data sets were measured from single crystals. Reflections were indexed, integrated, and scaled using the HKL software package (*25*). For both structures the space group was $C2$, with two molecules in the asymmetric unit, each containing 358 residues. The initial phasing model for the **2**/N289A structure was the **2**/WT AmpC complexed structure (PDB code 1MY8) with the ligand and solvent removed. The **2**/N289A structure without compound or solvent was then used as the initial phasing model for the **1**/N289A structure. Initial rigid body refinement was followed by positional minimization and B-factor refinement, using CNS (*26*). Sigma A-weighted electron density maps were calculated in CNS and used for manual corrections of the protein model and water placement in TURBO (*27*). The boronic acid inhibitors were fitted into positive $F_o − F_c$ density. In the **1**/N289A structure, the Asn → Ala substitution was visible as negative density in the $F_o − F_c$ density at position 289. Subsequent refinement cycles included compound and solvent and consisted of Cartesian and B-factor refinement in CNS. To create the wild-type/mutant crystal structure overlays (Figure 6), the two structures were matched at the Cα of all 358 residues of the B monomers using MidasPlus (*28*). The RMS errors were 0.19 Å for the structures with compound **1** and 0.17 Å for the structures with compound **2**.

Data Deposition. The coordinates and structure factors have been deposited in the Protein Data Bank under accession codes 1PI5 and 1PI4 for AmpC N289A in complex with compounds **1** and **2**, respectively.
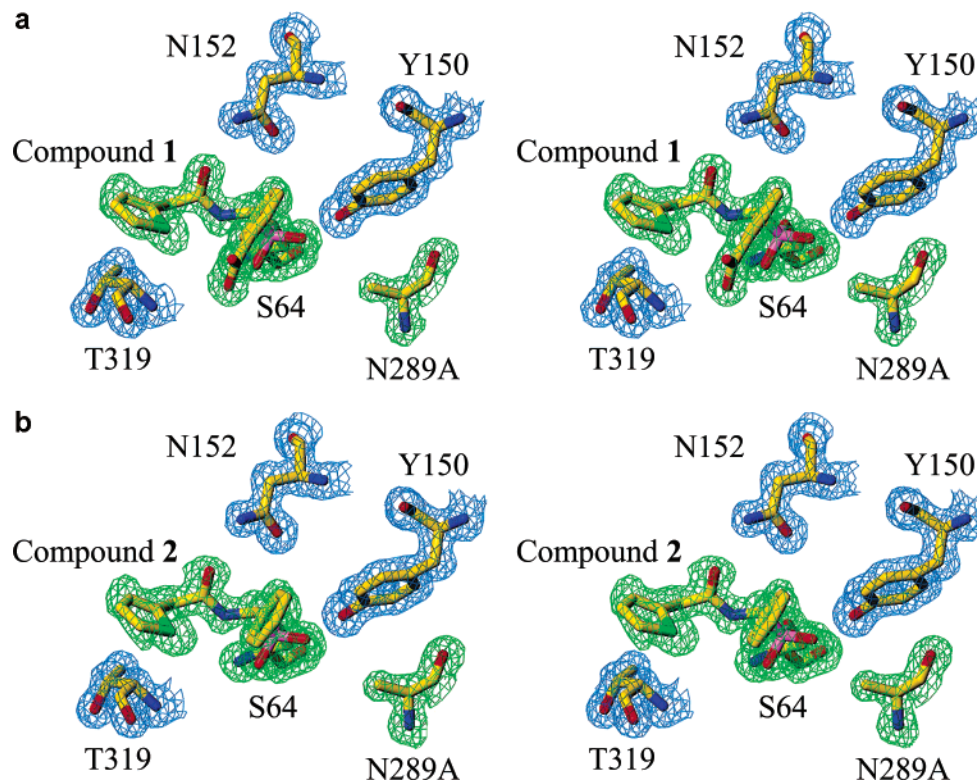
FIGURE 5: (a) Simulated annealing omit electron density of compound **1** in complex with N289A. The $F_o - F_c$ electron density (green) is contoured at 4σ. The $2F_o - F_c$ electron density (blue) is contoured at 1σ. (b) Simulated annealing omit density of compound **2** in complex with N289A. The $F_o - F_c$ electron density (green) is contoured at 4σ. The $2F_o - F_c$ electron density (blue) is contoured at 1σ.

Synthesis and Analysis of Compound 8. Compound **8** was synthesized as outlined in Scheme 1. All reactions were performed under argon using oven-dried glassware. Solvents were dried according to classical procedures. A cold bath at -100 °C was prepared by addition of liquid nitrogen to a precooled (-78 °C) mixture of 1:1 EtOH/MeOH. Chromatographic purification of the compounds was performed on silica gel (0.05–0.20 mm). Melting points were obtained on a Büchi 510 apparatus. Optical rotations were recorded at 20 °C on a Perkin-Elmer 241 polarimeter and are in 10^{-1} deg cm^2 g^{-1}. IR spectra were determined in KBr pellets (for solids) and films (for liquids) on a Perkin-Elmer 1600 series spectrophotometer. ^{1}H and ^{13}C NMR spectra were recorded on a Bruker DPX-200 (at 200 and 50 MHz, respectively) spectrometer: chemical shifts are reported in δ values from TMS as the internal standard. Mass spectra were determined on a Finnigan MAT SSQ A mass spectrometer (EI, 70 eV). Elemental analyses were performed on a Carlo Erba Elemental analyzer 1110.

1-Bromo-3-dimethoxymethyl-benzene (4b). Commercial 2-(3-Bromo-phenyl)-[1,3]dioxolane (1.3 mL, 8.64 mmol) was dissolved in anhydrous MeOH (40 mL) and catalytic amount of H$_2$SO$_4$ was added. The resulting reaction mixture was stirred 4 h at room temperature and finally extracted with petroleum ether (3 × 50 mL). The combined organic phases were washed with NaHCO$_3$ (40 mL), dried (MgSO$_4$), filtered and concentrated under vacuum to give **4b** as a colorless oil (1.76 g, 88%), whose spectroscopic data were in close agreement with literature (*29*).

(+)-Pinanediol (3-Dimethoxymethyl)phenylboronate (5b). *n*-BuLi (5.72 mL of a 2.5 M solution in hexane, 14.3 mmol) was added dropwise with stirring to a solution of **4b** (3.00 g, 13.0 mmol) in THF (8 mL) at -78 °C under argon. After

30 min, a solution of trimethylborate (1.50 mL, 13.0 mmol) in THF (4 mL) was added, and the mixture was stirred for 1.5 h. The resulting turbid solution was quenched with TMSCl (1.65 mL, 13.0 mmol) and allowed to reach rt. After 4 h a clear yellow solution is obtained and (+)-pinanediol (2.21 g, 13.0 mmol) dissolved in a minimum amount of anhydrous Et$_2$O was added and stirred overnight. The reaction mixture was partitioned in Et$_2$O (75 mL) and H$_2$O (25 mL), and the aqueous phase was extracted with Et$_2$O (3 × 25 mL). The combined organic phases were dried on MgSO$_4$, filtered, and concentrated to give an orange oil, which was purified by gradient chromatography (9:1 to 7:3 EtPet/EtOAc), affording **5b** (3.21 g, 75%) as a yellow liquid, $[\alpha]_D = +7.80$ (*c* 2.78, CHCl$_3$). ^{1}H NMR (CDCl$_3$): δ 0.88 (3H, s, pinanyl C*H*$_3$), 1.22 (1H, d, $J = 10.5$ Hz, pinanyl *H*$_{endo}$), 1.30 (3H, s, pinanyl C*H*$_3$), 1.47 (3H, s, pinanyl C*H*$_3$), 1.8–2.6 (5H, m, pinanyl protons), 3.33 (6H, s, CH(OC*H*$_3$)$_2$), 4.44 (1H, dd, $J = 8.8, 1.8$ Hz, pinanyl C*H*OB), 5.40 (1H, s, C*H*(OCH$_3$)$_2$), 7.37 (1H, t, $J = 7.6$ Hz, *H*$_5$ Ph), 7.55 (1H, d, $J = 7.6$ Hz, *H*$_6$ Ph), 7.78 (1H, d, $J = 7.6$ Hz, *H*$_4$ Ph), 7.90 (1H, s, *H*$_2$ Ph). ^{13}C NMR (CDCl$_3$): δ 25.4, 27.9, 28.5, 30.1, 36.9, 39.6, 40.9, 52.8, 54.1, 79.7, 87.6, 104.7, 129.0, 130.8, 134.5, 136.3, 138.8 (*C*B and aromatic quaternary *C* not seen). EIMS: *m/z* 330 (M$^+$), 315, 299 (base peak), 289, 261, 247, 203, 147, 121, 105, 93, 91, 83, 75, 67.

Following the same procedure, starting from **4a**, **5a** was obtained together with variable quantities of **5b** (5–50%). A careful gradient chromatography (9:1 to 1:1 EtPet/EtOAc) afforded an analitically pure sample of **5a** as a colorless oil that solidifies on standing, mp 47 °C, $[\alpha]_D = +8.01$ (*c* 2.12, CHCl$_3$). ^{1}H NMR (CDCl$_3$): δ 0.88 (3H, s, pinanyl C*H*$_3$), 1.22 (1H, d, $J = 10.5$ Hz, pinanyl *H*$_{endo}$), 1.31 (3H, s, pinanyl C*H*$_3$), 1.47 (3H, s, pinanyl C*H*$_3$), 1.7–2.5 (5H, m, pinanyl
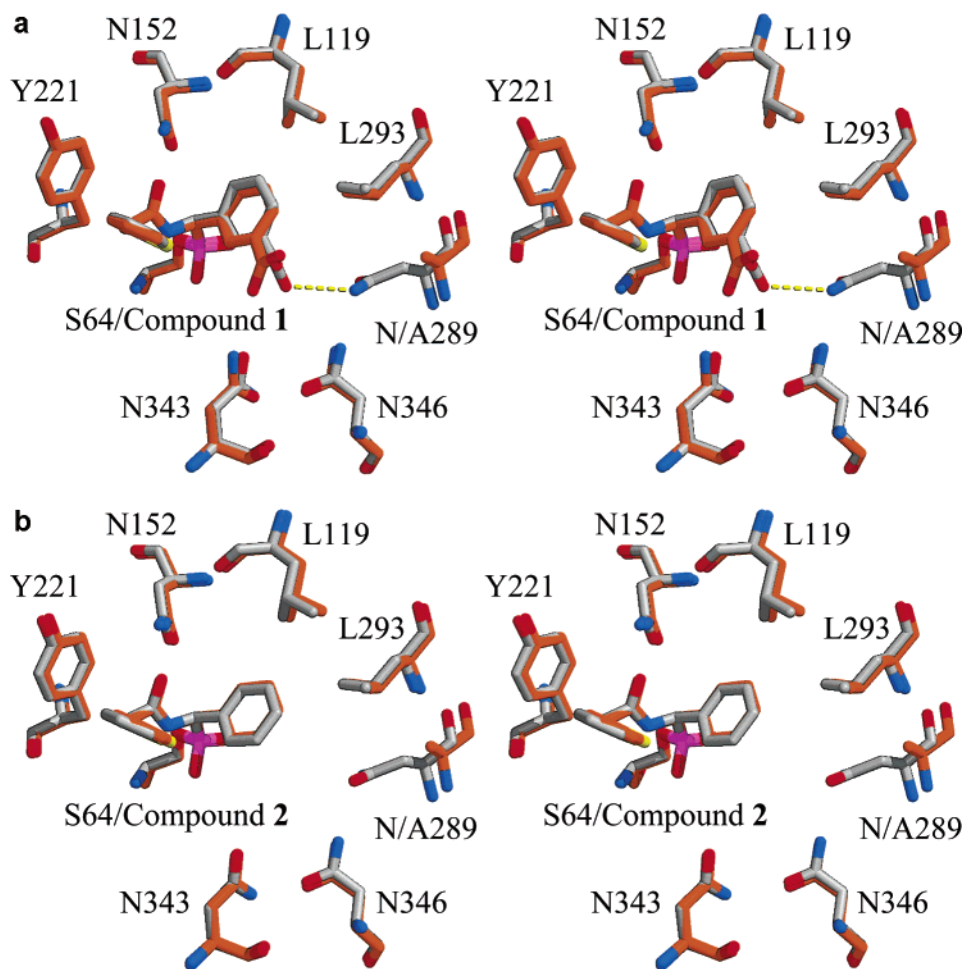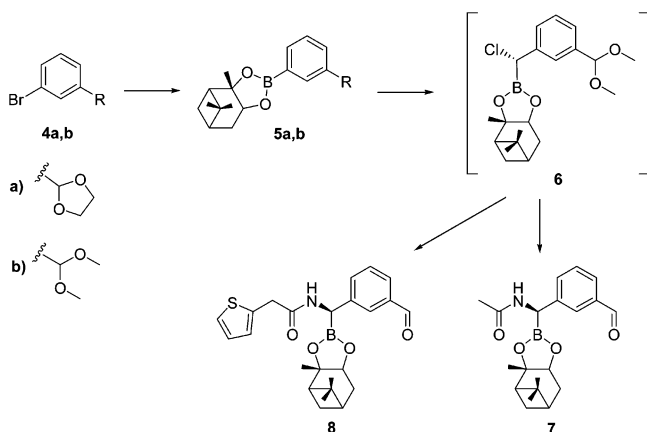
FIGURE 6: Overlay of wild-type and mutant enzyme complexes with compounds **1** and **2**. (a) Structures of **1**/WT AmpC (*10*) (carbons colored gray) and **1**/N289A (carbons colored orange). (b) Structures of **2**/WT AmpC (*10*) (carbons colored gray) and **2**/N289A (carbons colored orange).

Scheme 1: Steps in the Synthesis of Compound **8**

protons), 4.05 (4H, m, OCH_2CH_2O), 4.44 (1H, dd, $J = 8.8$, 1.8 Hz, pinanyl CHOB), 5.56 (1H, s, PhCHOCH$_2$), 7.39 (1H, t, $J = 7.7$ Hz, H_5 Ph), 7.58 (1H, dt, $J = 7.7$, 1.4 Hz, H_6 Ph), 7.83 (1H, dt, $J = 7.7$, 1.4 Hz, H_4 Ph), 7.94 (1H, s, H_2 Ph). ^{13}C NMR (CDCl$_3$): δ 25.4, 27.9, 28.5, 30.1, 36.9, 39.5, 40.9, 52.8, 66.7, 66.6, 79.7, 87.6, 105.2, 129.1, 130.6, 134.3, 137.0, 138.7 (CB not seen). EIMS: *m/z* 328 (M$^+$), 327, 312, 259, 232, 231, 215, 187, 149 (base peak), 105, 77, 73, 51.

General Procedure for the Synthesis of (+)-Pinanediol (1R)-1-Acylamino-1-(3-formylphenyl)methylboronate (7, 8). Dichloromethyllithium was generated by adding *n*-BuLi (1.82

mL of a 2.5 M solution in hexane, 4.6 mmol) dropwise to a solution of CH$_2$Cl$_2$ (0.43 mL, 6.6 mmol) in THF (15 mL) with stirring at -100 °C under argon: toward the end of the BuLi addition, precipitation of the white microcrystalline LiCHCl$_2$ became evident. After 30 min, the mixture was treated with the pinanediol boronate **5b** (1.368 g, 4.14 mmol) and allowed to reach 0 °C with stirring. The tetrahedral boronate adduct precipitated as a white solid at -80 °C and redissolved upon warming. After 1 h at 0 °C, the reaction mixture was partitioned between petroleum ether (150 mL) and H$_2$O (50 mL): the aqueous phase was extracted with petroleum ether (4 × 25 mL) and the combined organic phases were dried on MgSO$_4$, filtered and concentrated, giving the chloroderivative **6** as an orange oil (1.22 g, 78%), which was promptly used for the next step without further purification. (**6**) ^{1}H NMR (CDCl$_3$): δ 0.81 (3H, s, pinanyl CH_3), 1.13 (1H, d, $J = 10.5$ Hz, pinanyl H_{endo}), 1.27 (3H, s, pinanyl CH_3), 1.38 (3H, s, pinanyl CH_3), 1.6$-$2.5 (5H, m, pinanyl protons), 3.29 (6H, s, CH(OCH_3)$_2$), 4.36 (1H, dd, $J = 8.8$, 1.8, CHOB), 4.54 (1H, br s, ClCHB), 5.37 (1H, s, CH(OCH$_3$)$_2$), 7.25$-$7.38 (2H, m, H_5-H_6 Ph), 7.44 (1H, dt, $J = 6.3$, 1.8 Hz, H_4 Ph), 7.52 (1H, s, H_2 Ph).

(+)-Pinanediol (1R) 1-Acetylamino-1-(3-formylphenyl)- methylboronate (7). The crude chloro-derivative **6** (434 mg, 1.15 mmol) was dissolved in THF (4 mL) and cooled to -78 °C; LiN(TMS)$_2$ (1.15 mL of a 1 M solution in THF,

1.15 mmol) was added, and the resulting solution was allowed to warm gradually to 20 °C and stirred overnight. After 16 h at room temperature, the reaction mixture was cooled at −78 °C and treated with a solution of Ac$_2$O (0.435 mL, 4.6 mmol) and AcOH (79 μL, 1.38 mmol) in THF (2 mL), and then was allowed to warm to room temperature and stirred overnight. The solution was partitioned in EtOAc (40 mL) and H$_2$O (10 mL), and the aqueous phase was extracted with EtOAc (30, 20, 10 mL). The combined organic phases were washed with 5% NaHCO$_3$, dried over MgSO$_4$, and concentrated in vacuo to give an orange oil which was purified by chromatography (95:5 Et$_2$O/EtOH), affording **7** (50 mg, 12% overall yield from **5b**) as a pale yellow solid, mp 78−80 °C, $[\alpha]_D = -51.9$ (*c* 0.9, CHCl$_3$), de > 98%. IR (KBr): 1700, 1604 cm^{-1}. ^{1}H NMR (CDCl$_3$): δ 0.76 (3H, s, pinanyl C*H*$_3$), 1.15 (3H, s, pinanyl C*H*$_3$), 0.87 (1H, d, $J = 10.5$ Hz, pinanyl H_{endo}), 1.24 (3H, s, pinanyl C*H*$_3$), 1.6−2.4 (8H, m, pinanyl protons and C*H*$_3$CO at 2.18, s), 3.88 (1H, s, C*H*B), 4.05 (1H, dd, $J = 7.6$ Hz, C*H*OB), 7.3−7.5 (2H, m, H_5-H_6 Ph), 7.61 (1H, s, H_2 Ph), 7.68 (1H, d, $J = 7.6$ Hz, H_4 Ph), 8.8 (1H, br, N*H*CO), 9.96 (1H, s, C*H*O). ^{13}C NMR (CDCl$_3$): δ 25.4, 27.8, 28.6, 30.4, 37.9, 39.4, 41.3, 51.0 (br, *C*B), 53.8, 77.9, 67.2, 128.1, 130.2, 133.9, 137.8, 143.8, 177.4, 193.9. EIMS: *m/z* 355 (M$^+$), 286, 284, 259, 220, 205 (base peak), 178, 159, 149, 134, 105, 93, 83, 71, 57. Anal. Calcd for C$_{20}$H$_{26}$BO$_4$: C, 67.62; H, 7.38; N, 3.94. Found: C, 67.48; H, 7.30; N, 3.99.

(+)-Pinanediol (1R)-1-(2-Thienylacetylamino)-1-(3-form-ylphenyl)methylboronate (8). The crude chloroderivative **6** (602 mg, 1.6 mmol) was dissolved in THF (4 mL) and cooled to −78 °C; LiN(TMS)$_2$ (1.6 mL of a 1 M solution in THF, 1.6 mmol) was added, and the resulting solution was allowed to warm gradually to 20 °C and stirred overnight. After 16 h at room temperature, the reaction mixture was cooled at −78 °C, treated with a solution of 2-thiophenacetyl chloride (789 μL, 6.4 mmol) and 2-thiophenacetic acid (273 mg, 1.92 mmol) in THF (4 mL), and allowed to warm to room temperature stirring overnight. EtOAc (90 mL) and H$_2$O (15 mL) were added, and the aqueous phase was extracted with EtOAc (50, 20 mL). The combined organic phases were washed with 5% NaHCO$_3$, dried over MgSO$_4$, and concentrated in vacuo to give a brownish oil which was purified by gradient chromatography (100:0 to 90:10 Et$_2$O/MeOH), affording **8** (71 mg, 11% overall yield from **5b**) as a pale yellow solid, mp 68−70 °C, $[\alpha]_D = +5.0$ (*c* 7.2, CHCl$_3$), de > 98%. IR (KBr): 1698, 1601 cm^{-1}. ^{1}H NMR (CDCl$_3$): δ 0.78 (3H, s, pinanyl C*H*$_3$), 0.89 (1H, d, $J = 10.8$ Hz, pinanyl H_{endo}), 1.22 (3H, s, pinanyl C*H*$_3$), 1.30 (3H, s, pinanyl C*H*$_3$), 1.6−2.4 (5H, m, pinanyl protons), 3.95 (2H, s, C*H*$_2$-CO), 4.06 (1H, s, C*H*B), 4.16 (1H, dd, $J = 8.0, 2.0$ Hz, C*H*OB), 6.90−7.06 (2H, m, H_4 and H_3 thienyl), 7.27 (1H, m, H_5 thienyl), 7.32−7.50 (3H, m, H_6-H_5 Ph., N*H*CO), 7.59 (1H, s, H_2 Ph.), 7.66 (1H, m, H_4 Ph.), 9.91 (1H, s, C*H*O). ^{13}C NMR (CDCl$_3$): δ 25.4, 27.8, 28.6, 30.1, 35.0, 37.5, 39.5, 41.2, 48.5 (br, *C*B), 53.5, 78.4, 85.9, 126.2, 127.6, 128.6, 128.7, 129.0, 129.6, 130.3, 133.8, 143.3, 176.5 (*C*ONH), 193.8 (*C*OH). EIMS: *m/z* 438 (M+1), 437, 297, 285, 241, 220, 205, 201, 142, 11, 97 (base peak), 93, 71, 59. Anal. Calcd for C$_{24}$H$_{23}$BNO$_5$S: C, 65.91; H, 6.45; N, 3.20; S, 7.33. Found: C, 65.80; H, 6.33; N, 3.25; S, 7.17.

Table 1: K_i Values for Inhibitors

enzyme	inhibitor	K_i (nM)
WT AmpC	**1**	1[a]
WT AmpC	**2**	35[a]
WT AmpC	**3**	186
WT AmpC	**8**	15
AmpC N289A	**1**	17
AmpC N289A	**2**	37
AmpC N289A	**8**	18
AmpC L119A	**2**	12
AmpC L119A	**3**	676
AmpC L293A	**2**	521
AmpC L293A	**3**	6200

[a] From ref 10.

RESULTS

Enzymology and Binding Affinities. Three mutant AmpC enzymes were created to quantify interaction energies: Asn289 → Ala, Leu119 → Ala, and Leu293 → Ala. These substitutions were chosen to eliminate the interactions with the carboxylate and the phenyl ring of **1**, respectively, while minimizing the chance of introducing new interactions or perturbing the enzyme. All three mutant enzymes could be expressed and purified, although yields for L119A and L293A were lower than typical for wild-type. In the case of N289A, the relative stability of the folded enzyme, as determined by thermal denaturation using CD spectropola-rimetry, was nearly identical to that of wild-type (data not shown). All three enzymes retained substantial activity against β-lactam substrates such as nitrocefin. Both the "wild-type" and "mutant" inhibitors were tested against the corresponding enzymes of their respective thermodynamic cycles and K_i values were determined (Table 1).

Thermodynamic Cycle Analysis. The energy of the hydrogen bond between Asn289 and the carboxylate of compound **1** was investigated using the mutant enzyme N289A. This substitution reduced the affinity of **1** by 17-fold versus the wild-type enzyme (Table 1). The affinity of compound **2**, the decarboxy analogue of **1** (Figure 2b), falls 35-fold for the wild-type enzyme relative to the affinity of **1**, but only falls 2-fold for N289A relative to the affinity of **1** for the mutant. Construction of a double-"mutant" cycle reveals that the hydrogen bond between the carboxylate of **1** and the amide of Asn289 contributes 1.7 kcal/mol of net binding energy to the complex (Figure 4a). Similarly, the energy of the apparent nonpolar interaction between the phenyl ring of **2**, and by extension **1**, and the hydrophobic patch made up of Leu119 and Leu293 was investigated by the mutant enzymes L119A and L293A. Unexpectedly, the affinity of **2** for L119A was actually better than for the wild-type enzyme. Completion of the thermodynamic cycle by measuring the affinity of compound **3**, the achiral analogue of **2** that lacks the phenyl ring, gives a net interaction energy between the phenyl ring and L119 of −1.4 kcal/mol, i.e., this is an unfavorable interaction (Figure 4b). Although the L293 → Ala substitution does reduce the affinity for **2** by 1.6 kcal/mol, completing the same thermodynamic cycle suggests that here too the interaction with the phenyl ring is unfavorable, if only by −0.5 kcal/mol (Figure 4c).

The relatively high magnitude of the hydrogen bond between Asn289 and the carboxylate of **1** may be attributed to its ion−dipole character (*15*). Since the cost of desolvating

Table 2: Crystallography Statistics

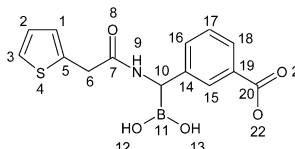| statistics	complex	
	N289A/**1**	N289A/**2**
cell constants (Å; deg)	$a = 119.05$; $b = 76.01$; $c = 97.60$; $\beta = 115.54$	$a = 118.63$; $b = 76.10$; $c = 97.84$; $\beta = 115.62$
space group	C2	C2
resolution range (Å)	15.0−1.49 (1.54−1.49)[a]	20.0−1.39 (1.45−1.39)[a]
unique reflections	128,092 (12,767)	156,947 (15,495)
total observations	483,237	903,131
R_{merge} (%)	5.1 (18.4)	5.8 (13.4)
completeness (%)	99.9 (100.0)	99.4 (98.3)
$\langle I \rangle / \langle \sigma(I) \rangle$	23.8 (7.6)	29.0 (10.4)
number of protein residues	716	716
number of water molecules	1179	1047
RMSD bond lengths (Å)	0.011	0.013
RMSD bond angles (deg)	1.61	1.71
R_{cryst} (%)	15.6	15.9
R_{free} (%)	16.9	17.3
average B-factor, protein atoms (Å^2)	14.5[b]	14.2[b]
average B-factor, inhibitor atoms (Å^2)	19.8[b]	15.3[b]
average B-factor, water molecules (Å^2)	31.8	29.0

[a] Values in parentheses are for the highest resolution shell. [b] Values cited were calculated for the B-monomer of the asymmetric unit.

the inhibitor carboxylate would be expected to be high (*30, 31*), we wondered what the affinity of a neutral hydrogen bond acceptor might be. To investigate this, the aldehyde analogue of **1**, compound **8** (Figure 2d), was synthesized. The affinity for wild-type AmpC was reduced 15-fold relative to that of **1**, whereas there was a negligible reduction in the affinity of **8** for N289A relative to that of **1**. Thermodynamic cycle analysis reveals that the hydrogen bond between Asn289 and the aldehyde is negligible. This is an example of an interaction where, notwithstanding the desolvation costs, an ionic interaction contributes significantly not only to specificity (*30, 31*) but also affinity.

X-ray Crystallographic Structure Determination. To understand the structural context of the hydrogen bond energy, the structures of the complexes of **1**/N289A and **2**/N289A were determined by X-ray crystallography to 1.48 Å for **1**/N289A and to 1.39 Å for **2**/N289A (Table 2). The two structures were refined to R_{cryst}/R_{free} values of 15.6/16.9% and 15.9/17.3%, respectively, and the overall statistics suggest well-determined structures (Table 2). The location of the inhibitors in the mutant enzyme, as well as the presence of the mutation itself, was determined by unambiguous simulated annealing omit electron density (Figure 5a,b). For both structures, 100% of the amino acids were either in the most favored regions or the additionally allowed regions of the Ramachandran plots (proline and glycine residues excluded). The interactions between the inhibitors and the enzyme are nearly identical to those between the inhibitors and wild-type AmpC (*10*), with the obvious exception of the lost hydrogen bond between the *m*-carboxylate of **1** and residue 289, now substituted by an alanine (Table 3). Overlays of the active sites of these two complexes with the corresponding wild-type complexes (*10*) demonstrate a close match (Figure 6a,b), indicating that there has been no significant reorganization of the active site in the mutant enzyme.

Synthesis. The synthesis of compounds **1**−**3** has been previously described (*9, 10*); (+)-pinanediol (1R)-1-acyl-amino-1-(3-formylphenyl)methylboronates **7**, **8** (Scheme 1) were obtained starting from commercial 2-(3-bromo-phenyl)-[1,3]dioxolane (**4a**), following the same procedure. Metalation of **4a** with buthyllithium at −78 °C, followed by reaction

Table 3: Key Enzyme−Inhibitor and Active Site Interactions Observed in the Crystal Structures

Compound **1**   Compound **2**

interaction	distance (Å)			
	1/N289A	**1**/WT AmpC[a]	**2**/N289A	**2**/WT AmpC[a]
S64N−O12	3.2	3.1	3.1	3.2
A318N−O12	2.8	2.7	2.8	2.8
A318O−O12	3.2	3.3	3.2	3.3
Y150OH−O13	2.6	2.7	2.6	2.7
Wat402−O12	3.0[b]	2.8	3.1	3.0
Wat402−O13	2.8[b]	3.0	2.9	2.9
Y150OH−K315Nξ	2.9	2.9	2.9	2.9
Y150OH−S64Oγ	3.1	3.0	3.1	3.0
Y150OH−K67Nξ	3.3	3.3	3.2	3.2
K67Nξ−A220O	2.9	2.8	2.9	2.9
K67Nξ−S64Oγ	2.8	2.6	2.8	2.7
Wat402−T316Oγ1	3.1[b]	3.4	3.1[c]	3.2
Wat402−Wat403	2.9[b]	2.6	2.8	2.7
Wat403−N346Oδ1	2.7	2.7	2.6	2.8
Wat403−R349Nη1	3.0	3.0	3.1	3.1
A318O−N9	3.1	3.1	3.1	3.2
N152Nδ2−O8	2.9	2.8	2.9	2.9
Q120Nε2−O8	3.5	6.5	3.4	2.9
N152Oδ1−K67Nξ	2.7	2.6	2.7	2.6
N152Nδ2−Q120Oε1	3.0	7.1	3.1	2.6
Wat181−O22	2.4	3.0	NP	NP
Wat469−O23	NP[d]	3.1	NP	NP
N289Nδ2−O22	NP	2.9	NP	NP

[a] From ref 10. [b] Denotes value for one of two conformations of equal occupancy. [c] Denotes value for conformation with highest occupancy. [d] NP: not present.

with trimethylborate and transesterification with (+)-pinanediol, afforded the desired (+)-pinanediol (3-[1,3]dioxolan-2-yl-phenyl)boronate (+)-**5a** together with a variable amount of (+)-pinanediol (3-dimethoxymethyl)phenylboronate (+)-**5b**, this latter probably formed by transacetalization with the in situ formed methanol. To avoid this problem,

4a was converted to **4b** (88%) and subsequently boronated to (+)-**5b** (75%).

Boronate (+)-**5b** was converted to compound **6** employing the described procedure for Matteson homologation (*32, 33*). (+)-Pinanediol as chiral auxiliary is known to guide the stereochemical course of the homologation reaction (*34, 35*) affording the α-chloro derivative **6** in the desired *S* configuration. To prevent epimerization (*32, 33*), this compound was used for the next step without purification and rapidly converted to the acylamino boronic ester in a one-pot procedure that involved substitution with bis-trimethylsilyllithium amide, acylation (acetic anhydride or thienyl acetyl chloride), and aldehyde deprotection (10−12% overall yield from **5b**). Compound (1*R*)-(−)-**7** and (1*R*)-(+)-**8** showed ¹H and ¹³C NMR, IR, mass spectra, and elemental analyses in close agreement with the desired structures; high diastereoisomeric purity (de > 98%) was displayed by diagnostic signals in ¹H NMR analysis (*36, 37*).

DISCUSSION

A key result to emerge from these studies is the large magnitude of the interaction energy between the amide of Asn289 and the carboxylate of the inhibitor **1**. The 1.7 kcal/mol contributed by this hydrogen bond to overall affinity is within the range observed for ion−dipole hydrogen bonds between substrate groups and conserved recognition residues in enzymes (*15*). The importance of the ionic character of this interaction, as attested to by the effect of compound **8**, is less expected; it is an example of a charged group contributing not only to specificity but also affinity, notwithstanding the desolvation cost (*30, 31*). What is most surprising is that Asn289 is *not* a conserved recognition residue among the class C β-lactamases (*38−40*), nor is it known to play an important role in substrate recognition (*10*). Thus, whereas the energy that this interaction contributes to binding may be justified biophysically, its origins are in some sense an accident of sequence variation in AmpC. What then are the implications for inhibitor design in this series?

Were this a human target, we would waste no anxiety on the fortuitousness of this interaction. Indeed, a happy implication of this work is that one can hope to find strong binding interactions even outside of canonical recognition residues. Unfortunately, antimicrobial chemotherapy unhorses so cavalier an idea: we are not only interested in AmpC from *Escherichia coli* but also in the class C β-lactamases from other pathogens, and in these residue 289 is often not an asparagine. For instance, in the *Enterobacter cloacae* enzyme residue 289 is a serine, and for this enzyme the affinity of **1** is only 29 nM (not shown). To design an inhibitor that has a broad spectrum of action across species and resists mutations of the targets, it will be necessary to target future derivatives toward less labile parts of the active site. Examples might include the canonical carboxylate recognition residues in AmpC, including Asn343 and Asn346 (*11, 38*), which are quite close in space to the carboxylate of **1**, and may well be accessible.

The thermodynamic cycles probing the interactions between the phenyl ring of **1** and the leucine patch on AmpC (Figure 4b,c) will also guide future inhibitor design. Structural and computational studies have suggested that this exposed hydrophobic patch is a good target for inhibitor groups to complement (*11*). On the basis of the observation that the phenyl ring in **1** and **2** are in close contact with this patch in the enzyme complexed structures determined by crystallography (*10*), we had expected that the interaction between the inhibitor and residues would be favorable. In fact, it is not. Although having a phenyl ring in **1** and **2** improves binding, this does not owe to interactions with residues with which it interacts most closely. The explanation for this may be that the phenyl ring interacts with other nearby residues, such as Gln120, which appears to form a quadrupole−dipole interaction with the phenyl ring, or that the hydrophobicity of the phenyl ring is largely responsible for its contribution to affinity. If this is true, it would suggest that the exact nature of this hydrophobic group is relatively unimportant, as long as it provides a good spacer for delivering the carboxylate or analogous anion to the active site.

We return to the use of thermodynamic cycles in inhibitor design. Here, double perturbation analysis reveals that interactions that appeared important based on affinity changes and X-ray crystal structures were energetically fortuitous. One thus might question whether we are any closer toward a good lead for drug design, having undertaken this study. We contend that these results are critical to such design. In the absence of this analysis, we would conclude that the carboxylate on **1** is a critical feature of future design and should be maintained; after all, deleting this group (as in **2**) reduces affinity by 35-fold. These studies suggest that this contribution, though undisputable, owes largely to an interaction with a nonconserved residue. Future inhibitors may do well to deploy anionic functionality against other, albeit nearby, groups in the active site. Similarly, whereas the phenyl ring of **1** and **2** interacts with a conserved hydrophobic patch in class C β-lactamases, and whereas this phenyl ring contributes an order of magnitude binding affinity to these inhibitors, the structurally observed interaction with the leucine patch is not responsible for this increase in affinity. It may be useful to target other parts of the binding site in subsequent design efforts. More generally, this study supports the view that "rational" inhibitor design cannot be based on structure alone, as powerful as that is, but must ultimately consider the detailed energetic bases of affinities. This has long been recognized in substrate (*15*) and ligand recognition studies (*19*); the technique provides exciting opportunities for "rational" design as well.

ACKNOWLEDGMENT

REFERENCES

1. Neu, H. C. (1992) *Science 257*, 1064−1073.
2. Davies, J. (1994) *Science 264*, 375−382.
3. Baquero, F., and Blazquez, J. (1997) *Trends Ecol. Evol. 12*, 482−487.
4. Matagne, A., Dubus, A., Galleni, M., and Frere, J. M. (1999) *Nat. Prod. Rep. 16*, 1−19.

5. Sutherland, R. (1991) *Trends Pharmacol. Sci. 12*, 227−232.
6. Usher, K. C., Blaszczak, L. C., Weston, G. S., Shoichet, B. K., and Remington, S. J. (1998) *Biochemistry 37*, 16082−16092.
7. Weston, G. S., Blazquez, J., Baquero, F., and Shoichet, B. K. (1998) *J. Med. Chem. 41*, 4577−4586.
8. Powers, R. A., Blazquez, J., Weston, G. S., Morosini, M. I., Baquero, F., and Shoichet, B. K. (1999) *Protein Sci. 8*, 2330−2337.
9. Caselli, E., Powers, R. A., Blaszczak, L. C., Wu, C. Y., Prati, F., and Shoichet, B. K. (2001) *Chem. Biol. 8*, 17−31.
10. Morandi, F., Caselli, E., Morandi, S., Focia, P. J., Blazquez, J., Shoichet, B. K., and Prati, F. (2003) *J. Am. Chem. Soc. 125*, 685−695.
11. Powers, R. A., and Shoichet, B. K. (2002) *J. Med. Chem. 45*, 3222−3234.
12. Beadle, B. M., Trehan, I., Focia, P. J., and Shoichet, B. K. (2002) *Structure 10*, 413−424.
13. Patera, A., Blaszczak, L. C., and Shoichet, B. K. (2000) *J. Am. Chem. Soc. 122*, 10504−10512.
14. Powers, R. A., Caselli, E., Focia, P. J., Prati, F., and Shoichet, B. K. (2001) *Biochemistry 40*, 9207−9214.
15. Fersht, A. R. (1999) *Structure and Mechanism in Protein Science*, W. H. Freeman and Company, New York.
16. Horovitz, A. (1987) *J. Mol. Biol. 196*, 733−735.
17. Albeck, S., Unger, R., and Schreiber, G. (2000) *J. Mol. Biol. 298*, 503−520.
18. Frisch, C., Schreiber, G., Johnson, C. M., and Fersht, A. R. (1997) *J. Mol. Biol. 267*, 696−706.
19. Ranganathan, R., Lewis, J. H., and MacKinnon, R. (1996) *Neuron 16*, 131−139.
20. Carter, P. J., Winter, G., Wilkinson, A. J., and Fersht, A. R. (1984) *Cell 38*, 835−840.
21. Bradshaw, J. M., Mitaxov, V., and Waksman, G. (1999) *J. Mol. Biol. 293*, 971−985.
22. Willcockson, I. U., Hong, A., Whisenant, R. P., Edwards, J. B., Wang, H., Sarkar, H. K., and Pedersen, S. E. (2002) *J. Biol. Chem. 277*, 42249−42258.
23. Ho, S. N., Hunt, H. D., Horton, R. M., Pullen, J. K., and Pease, L. R. (1989) *Gene 77*, 51−59.
24. Waley, S. G. (1982) *Biochem. J. 205*, 631−633.
25. Otwinowski, Z., and Minor, W. (1997) *Methods Enzymol. 276*, 307−326.
26. Brunger, A. T., Adams, P. D., Clore, G. M., DeLano, W. L., Gros, P., Grosse-Kunstleve, R. W., Jiang, J. S., Kuszewski, J., Nilges, M., Pannu, N. S., Read, R. J., Rice, L. M., Simonson, T., and Warren, G. L. (1998) *Acta Crystallogr. D 54*, 905−21.
27. Cambillau, C., and Roussel, A. (1997) Turbo Frodo; OpenGL ed.: Universite Aix-Marseille II, Marseille, France, 1997.
28. Ferrin, T. E., Huang, C. C., Jarvis, L. E., and Langridge, R. (1988) *J. Mol. Graph. 6*, 13−27.
29. Yu, R., Yakimansky, A., Voigt-Martin, I. G., Fetten, M., Schnorpfeil, C., and Schollmeyer, D. (1999) *J. Chem. Soc., Perkin Trans. 2*, 1881−1890.
30. Hendsch, Z. S., Jonsson, T., Sauer, R. T., and Tidor, B. (1996) *Biochemistry 35*, 7621−7625.
31. Luisi, D. L., Snow, C. D., Lin, J. J., Hendsch, Z. S., Tidor, B., and Raleigh, D. P. (2003) *Biochemistry 42*, 7050−7060.
32. Matteson, D. S., Ray, R., Rocks, R. R., and Tsai, D. J. (1983) *Organometallics 2*, 1536−1543.
33. Matteson, D. S. (1988) *Acc. Chem. Res. 21*, 294−300.
34. Matteson, D. S. (1989) *Chem. Rev. 89*, 1535−1551.
35. Matteson, D. S. (1999) *J. Organomet. Chem. 581*, 51−65.
36. Tsai, D. J. S., Jesthi, P. K., and Matteson, D. S. (1983) *Organometallics 2*, 1543−1545.
37. Matteson, D. S., Sadhu, K. M., and Peterson, M. L. (1986) *J. Am. Chem. Soc. 108*, 810−819.
38. Lobkovsky, E., Billings, E. M., Moews, P. C., Rahil, J., Pratt, R. F., and Knox, J. R. (1994) *Biochemistry 33*, 6762−6772.
39. Carfi, A., Pares, S., Duee, E., Galleni, M., Duez, C., Frere, J. M., and Dideberg, O. (1995) *EMBO J. 14*, 4914−4921.
40. Massova, I., and Mobashery, S. (1998) *Antimicrob. Agents Chemother. 42*, 1−17.